Pergamon

Journal of Structural Geology, Vol. 18, Nos 2/3, pp. 179 to 190, 1996

0191-8141/96 $15.00+0.00

0191-8141(96)00107-7

Properties of fault populations in the Gullfaks Field, northern North Sea

HAAKON FOSSEN

Statoil, GF/PETEK-GEO, N-5020 Bergen, Norway

and

ASTRI RØRNES

Statoil, N-7005 Trondheim, Norway

(*Received* 9 *January* 1995; *accepted in revised form* 21 *August* 1995)

Abstract—There are many published examples of the size–frequency distributions of natural fault populations that have been interpreted as showing scale-invariant power-law scaling. In this paper we present the statistics of the fault throw population in the Gullfaks Field and show that the distribution can not be described by a single power law. Instead, the throw population, when plotted in log–log space, displays two distinct slopes with different exponents at scales well above the limit of seismic resolution. At scales ranging from 10 to 90 m we obtained a slope of approximately 0.3, while at scales ranging from 90 to 165 m the slope is approximately 1.0. A systematic variation in fault orientation with fault size does not appear to be the cause of this break in slope, and a simple explanation has yet to be found. However, the documentation of such a change in scaling above seismic resolution implies that similar breaks may occur equally well below the resolution limit. This suggests that extrapolation of the straight line segments of population curves to sub-seismic scales may give incorrect estimates of small-scale faults and fractures.

Separation of the Gullfaks fault data set into subareas and sub-populations, based on geometric criteria, revealed several sub-populations of faults that do exhibit simpler power-law relationships. However, the wide range of values found for the scaling exponent (varying from 0.73 to 2.05) suggests that the choice of such subdivisions is an important step in the analysis procedure. We argue here that a more thorough understanding of fault populations can be achieved by documenting this sub-population variability as well as by characterizing the combined data set.

INTRODUCTION

Fault populations from the North Sea and other extensional areas have been described as exhibiting power-law or fractal size distributions (e.g. Hirata 1989, Kojima *et al.* 1989, Childs *et al.* 1990, Peacock & Sanderson 1994). It has been proposed that if a power-law distribution can be established for a certain interval of a data set (e.g. above seismic resolution for seismically derived data), the same scaling property can be extrapolated outside of the interval in question (e.g. to predict faults smaller than the seismic resolution) (Walsh *et al.* 1991, Marrett & Allmendinger 1992, Yielding *et al.* 1992, Gauthier & Lake 1993). However, a growing amount of mostly unpublished data (e.g. Brodahl 1993) indicates that even though many data sets show a power-law size distribution over a certain range in scale, this distribution does not necessarily extend over several orders of magnitude, i.e. the population is not truly scale invariant.

These issues will be discussed in the following analysis of data collected from the extensional fault system of the Gullfaks Oil Field, northern North Sea. More than 130 exploration and production wells have been drilled on this field during the last 20 years, and a large amount of log-data, core material and three-dimensional seismic data have been collected before and after production was initiated in 1986. The existing data base forms a unique collection of structural and stratigraphic data from an area of simple extensional deformation, and has been used to analyse the fault population statistics in the area.

STRUCTURAL SETTING

Regional setting

The northern North Sea is generally believed to have been influenced by at least two main phases of extension (e.g. Badley *et al.* 1988) after the thinning and regional stretching of the thickened Caledonian crust in the Devonian (see Fossen 1992 for a more detailed discussion of this topic). The first of these is a Permo-Triassic phase that is poorly defined on seismic data from the northern North Sea (cf. Roberts *et al.* 1995). The Viking Graben was established during this phase, and was later overprinted by a roughly E–W-stretching phase in the latest Middle Jurassic to earliest Cretaceous (Roberts *et al.* 1990) (Fig. 1). The faults studied in this work occur in Jurassic rocks, and are thus a product of the latter extension phase only.

A regional unconformity separates faulted and

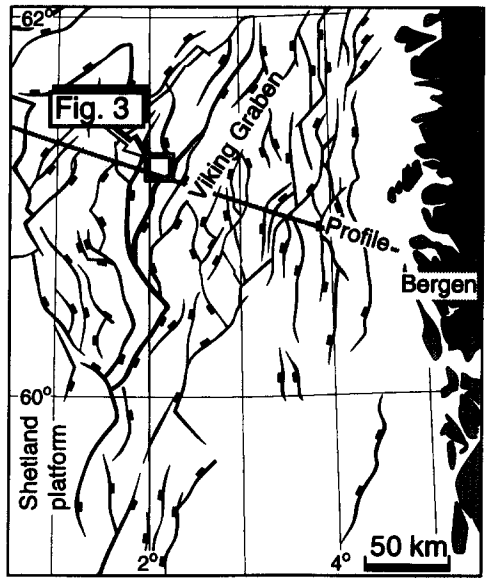

Fig. 1. Location of the study area in the North Sea rift.

rotated Triassic and Lower–Middle Jurassic sediments from mainly unfaulted and flat-lying Cretaceous and later deposits (Fig. 2b). This unconformity represents a time gap of up to 100 Ma on structurally high areas like the Gullfaks Field. The post-Jurassic history of the North Sea is characterized by basin subsidence and continuous sedimentation.

The Gullfaks Field

The Gullfaks oil field (Erichsen *et al.* 1987, Petterson *et al.* 1990) is situated on the western side of the North Sea Rift System in the Norwegian sector of the northern North Sea (Fig. 1). The reservoir units are located within heavily faulted late Triassic and Lower–Middle Jurassic sediments. The Triassic–Jurassic stratigraphy of the Gullfaks Field comprises alternating alluvial–fluvial sands and shales of the Lunde and Statfjord Formations (Upper Triassic to Lower Jurassic), the partly marine Dunlin Group (Lower Jurassic) and the deltaic Brent Group (Middle Jurassic).

Structurally, the Gullfaks Field forms the eastern part of a 10–25 km wide, first-order Late Jurassic fault block close to the Viking Graben axis (Fig. 2a). The Gullfaks oil field can be subdivided into a western domino system, an eastern, elevated horst complex, and an intermediate accommodation zone (Fig. 2b).

The domino area is characterized by a series of roughly N–S-striking faults with 50–500 m throw, all dipping 25–30° to the east. These faults define a series of domino-style fault blocks that are tilted about 15° to the west. The domino blocks are compartmentalized by variably-oriented smaller faults, of which most have throw <80 m. These minor faults are generally confined to single domino blocks.

The horst complex is bounded to the east by a first-order fault with km-scale throw down towards the Vik-

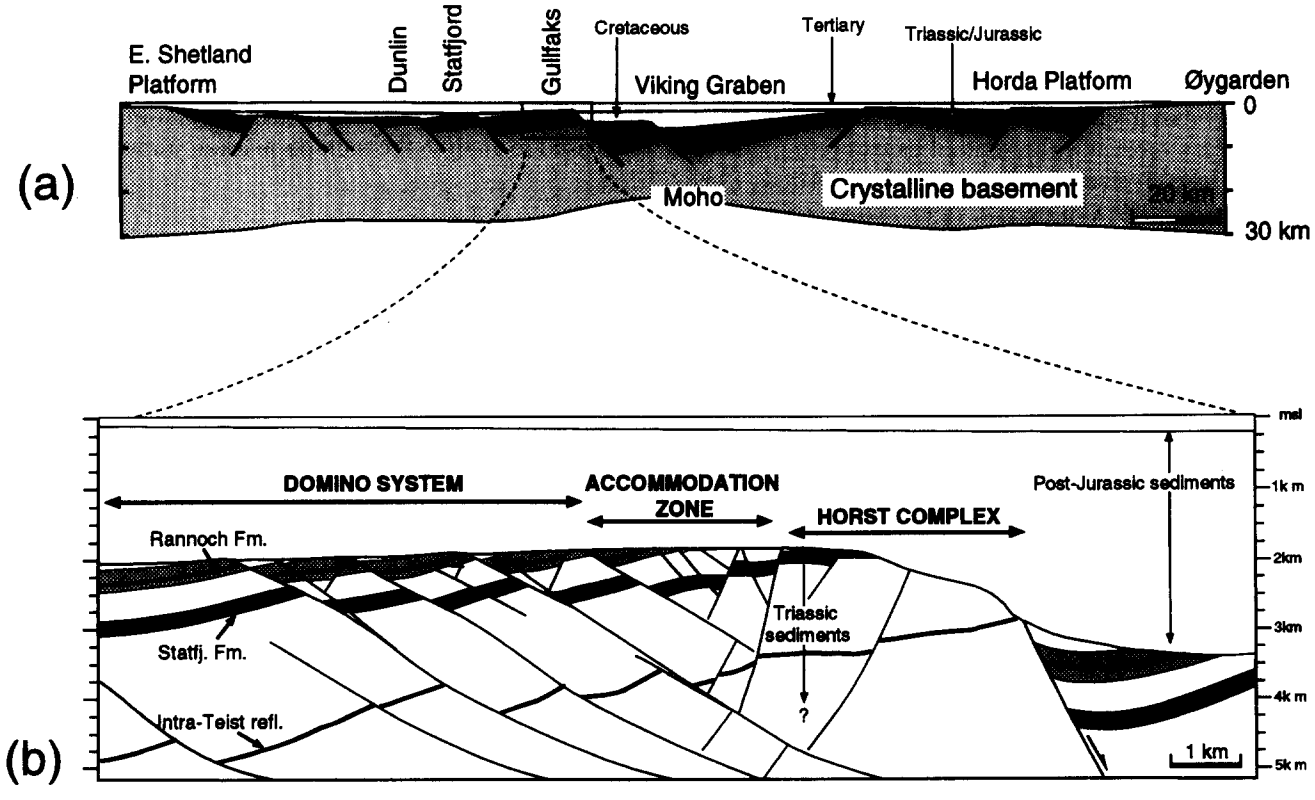

Fig. 2. (a) Regional profile across the North Sea and Gullfaks Field (after Marsden *et al.* 1990). See Fig. 1 for location. The Gullfaks Field is located on the western side of the Viking Graben, and is bounded by an E-dipping, first-order normal fault. (b) Detailed cross-section of the Gullfaks area, showing the geometry of the western domino system, the horst complex and the intermediate accommodation zone.

ing Graben. This complex represents an area of deep Late Jurassic–Cretaceous erosion, and forms the structurally highest point in the area. The horst complex is characterized by horizontal bedding and steeper (60–65°) faults than in the domino area.

The accommodation zone is defined by a gentle fold structure where the western limb dips 15–20° to the west, and the eastern limb is subhorizontal to gently E-dipping. The fold structure is affected by several minor faults indicating extensional collapse of its outer arc. The deformation in this zone accommodates the different deformation styles in the horst complex and the domino area. This use of the word accommodation zone should not be confused with definitions given by other authors, for example Scott & Rosendahl (1989).

FAULT CLASSIFICATION

For detailed analysis of size distributions, fault populations may be subdivided or classified with respect to genetic or geometric criteria (Gauthier & Lake 1993), or simply by geographic subdivision into regular subareas (Yielding *et al.* 1992). Useful genetic criteria include timing or sequence of faulting (different deformations), type of faulting (reverse, strike-slip or normal) and their relation to deformation mode (pre-rift, syn-rift, gravity-driven or compaction-related, or tectonic). Geometrically, fault populations can be subdivided based on differences in strike, dip or dip direction. In general, geometric criteria are easier to handle in an objective way than are genetic criteria.

Stratigraphic evidence and the structural configuration of the Gullfaks Field indicate that all the mapped faults formed more or less at the same time during the Late Jurassic rifting phase of the North Sea Rift System. It has already been pointed out that the Gullfaks area can be subdivided into three geometrically as well as genetically different areas, namely the domino system, the horst area and the accommodation zone (see above).

Within the domino system, the main faults are a direct product of the regional, Late Jurassic, extension, whereas some of the internal, E–W-striking faults are best understood as contemporaneous adjustment faults accommodating differential slip along the main faults during the same extension phase. Minor, NW- through to NE-striking conjugate faults indicate an extensional collapse of the gentle fold structure in the accommodation zone. The horst complex is not treated in this work because of the scarcity of reliable data from this deeply-eroded part of the field. Further subdivision of the faults within the domino system and the accommodation zone can be done based on variations in strike and dip direction.

FAULT ANALYSIS

Method and data collection

For fault populations where the variation in frequency N with variation in size S (e.g. throw size) follows a power law, the relationship can be expressed in the form

$$N = aS^{-D}$$

or

$$\log N = \log a - D \log S,$$

where the exponent D describes the fractal dimension of the population or the slope of the straight line that appears for such populations in a log–log plot of cumulative frequency against size, and a is a constant (see Childs *et al.* 1990, Marrett & Allmendinger 1992, or Gauthier & Lake 1993 for a more thorough introduction to this subject).

Size attributes of faults that are most commonly studied are fault lengths (measured from a two-dimensional data set such as a map) and fault throws (often measured along one-dimensional profiles or from cross-sections). Objective fault length analysis is practically impossible on Gullfaks, because of the highly interconnected nature of the fault population. The present study is therefore restricted to throw analyses represented by multi-line population curves, in which throw readings from a number of parallel profile lines are combined (see Walsh *et al.* 1994 for a detailed discussion of this method).

Multi-line data were collected from detailed three-dimensional interpretation of well-defined Jurassic reflectors corresponding to or lying close to the top of the Rannoch Formation of the Brent Group and the top of the Stratfjord Formation. (Figs 3–5). Additional stratigraphic and dipmeter data from some 150 wells that penetrate or are close to these two reflectors help constrain the seismic interpretation, which involved existensive use of seismic attribute analysis. Faults were manually recorded at a seismic work station on the depth-converted interpretation, and entered into a spread-sheet for structural analysis. A total number of 64 lines (regularly spaced E–W profiles, 200 m apart) corresponding to 510 km (at Rannoch level) and 675 km (at Statfjord level) of profile length were collected. In addition, data were collected along 24 N–S profiles located 437.5 m apart (totalling 240 km for Rannoch, and 315 km for top Statfjord). More extensive erosion of the Rannoch Formation compared to the Statfjord Formation (Fig. 2b) causes the differences in length. The more complete sampling of the Statfjord Formation makes it a better candidate for fault population studies. Hence, most of the results presented below are for the Statfjord Formation.

Local drag immediately around the faults can be observed in Gullfaks. Core and dipmeter data analyses show that local deflection of the bedding in zones less than 70 m from the faults is 'true' drag (micro-scale deformation), and not an expression of meso-scale faulting or fracturing. Seismic expression of drag is less obvious from the seismic data, although it can be observed in several places. Ductile drag has been a problem in some of the previous work on fault populations, particularly where onshore data have been used (Walsh

& Watterson 1987). However, this problem has been eliminated in the present study, since the recorded displacements always include both the discrete offset and the more 'ductile' offset represented by local drag.

Total population, Gullfaks Field

The total fault population from the area covered by Fig. 3 (Statfjord Formation) was plotted as a multi-line population curve in a log–log plot as shown in Fig. 6. The result is a bi-linear or segmented curve, leading to the interpretation that the population is not scale invariant. The characteristic left-hand, shallow segment for the range of data below the typical seismic resolution (*ca* 15 m) and the right-hand, steep segment also ascribed to sampling artifacts (Yielding *et al.* 1992) are recognizable. Between these upper and lower limits, it is possible to identify two sub-linear intervals with different slopes. One is for throws between 90 and 165 m (slope about −1.07), the other is for the range 10–90 m (slope of −0.3). Within these restricted intervals the population does exhibit power-law distributions, particularly at the Statfjord level. Because the large fault east of the Gullfaks Field is not included in this data set it is likely that these slopes are overestimated. This is caused by undersampling the largest faults in a region, an effect termed *censoring* and further discussed by Jackson & Sanderson (1993). Adding a fault with 1 km of throw to each of our line samples changed the slopes to −0.95 and −0.27, respectively.

The relatively well-defined break in slope (Fig. 6a) at 90 m indicates that the two populations related to the two straight segments do not have a large overlap. A closer look at Fig. 3 reveals a fundamental difference in orientation between the N–S-striking faults, which generally have throws greater than 90 m, and the more irregular but generally E–W-trending faults which have throws less than about 90 m. The result of such a systematic difference in orientation between large and small faults may have a significant impact on log–log plots like Fig. 6. Sampling was performed along lines perpendicular to the N–S-striking main faults, in accordance with the technique suggested by Walsh *et al.* (1994).

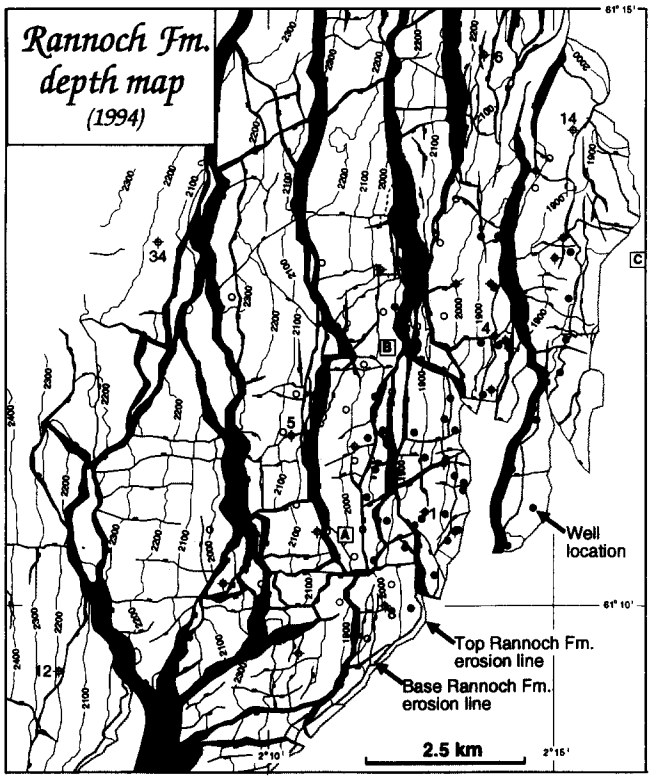

Fig. 4. Depth structure contour map of the Middle Jurassic Rannoch Formation of the Brent Group, Gullfaks Field. Exploration wells are numbered. Filled/open well symbols indicate oil/no oil in the Rannoch Formation. Open symbols with a cross indicate injector. Filled well symbols indicate oil in reservoir. Contour interval is 100 m.

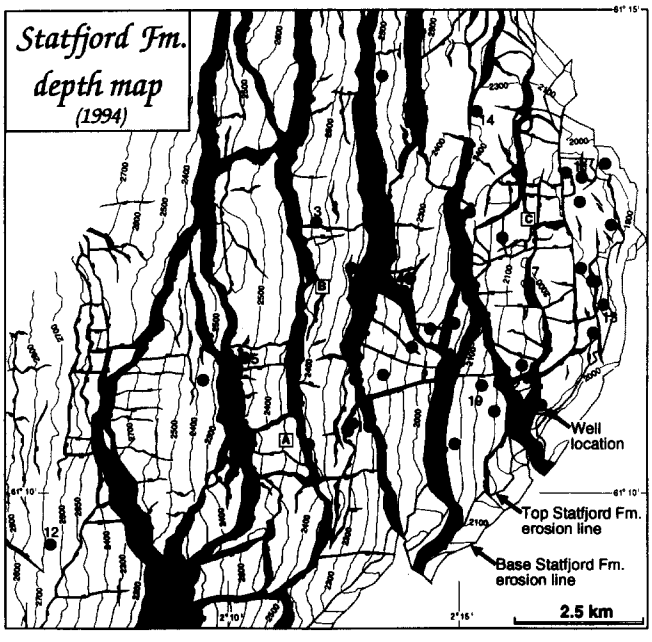

Fig. 3. Depth structure contour map of the Lower Jurassic Statfjord Formation in the Gullfaks Field area. Exploration wells are numbered. Contour interval is 100 m.

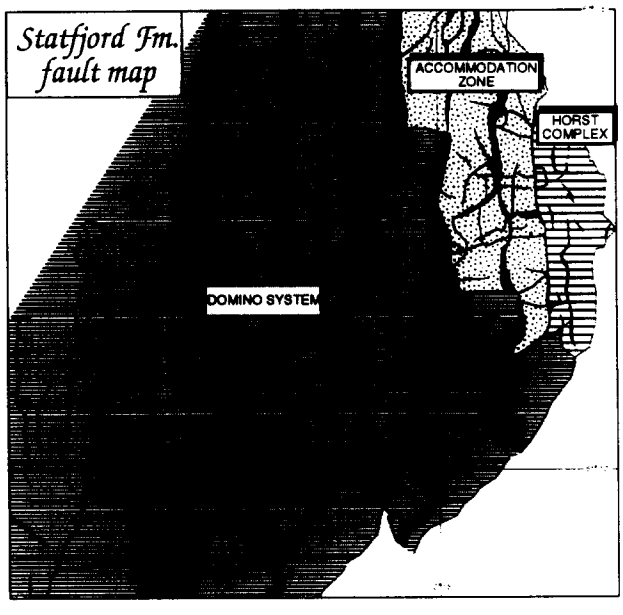

Fig. 5. Distribution of the three structural sub-areas shown in Fig. 2(b).

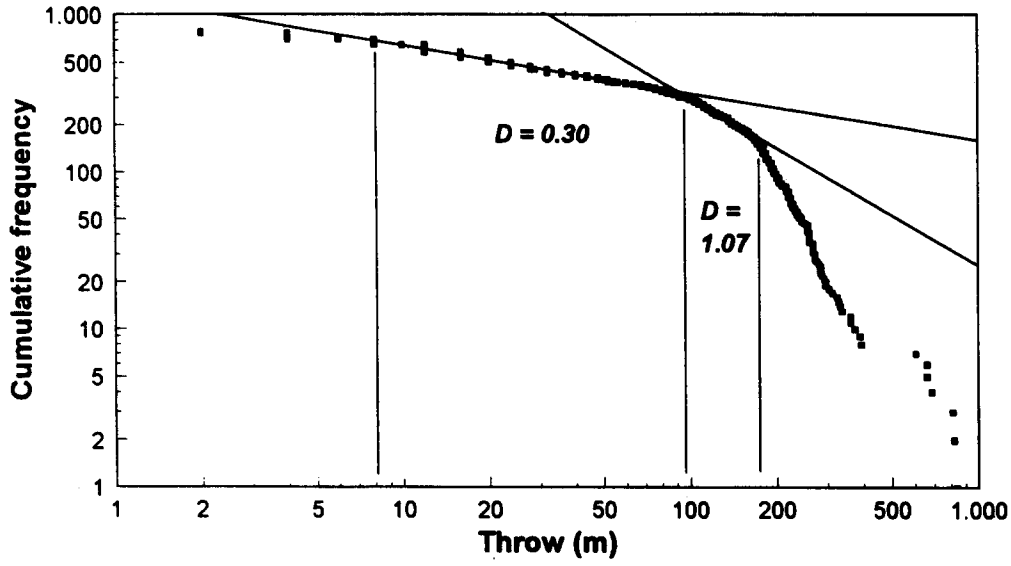

Fig. 6. Cumulative frequency–throw plot (multi-line log–log population curve from 64 E–W lines) for the entire fault population mapped in the area covered by Fig. 3 (Statfjord Formation). Two straight segments are recognized with a change in slope from −0.3 to −1.07 at about 80–100 m in addition to the shallowly (left-hand side) and steeply dipping (right-hand side) characteristic tails. The slopes are fitted by the least squares method for the ranges defining (semi-) straight curve segments (indicated by vertical lines). See text for discussion.

Consequently, E–W faults will be heavily under-represented, and either a segmented log–log curve (Fig. 6) or a curve without straight segments may be expected.

To further investigate this orientation effect, data from a series of N–S lines were collected to sample the additional E–W-trending faults. In this way all the mapped faults were sampled either along N–S or E–W profiles, and the combined data set was plotted (Fig. 7). Since the number of small faults is larger in this data set, the left-hand part of the curve (throw < 50–90 m) has steepened (D has changed from 0.3 in Fig. 6 to 0.4 in Fig. 7). However, there is still a break in slope at about 90–100 m throw.

A similar exercise can be done using well information. Detailed log correlation makes it possible to detect faults and the amount of missing stratigraphic section in each of the many wells on the Gullfaks Field. This information can be plotted in log–log diagrams where throw in Fig. 7 is replaced with missing section (equal for the case of horizontal bedding). These well data represent an independent source of data, and the result is shown in Fig. 8.

Before comparing Fig. 8 with the result from the seismic data, the differences in collection should be discussed. The wells are drilled in a variety of directions and with different inclinations (some are vertical, but most are deviated, and some are horizontal in the Triassic–Jurassic reservoir section). The population slopes therefore cannot directly be correlated with the ones in Fig. 6. However, because of the variation in well azimuth (varying from E–W to N–S), the orientation effects related to differences in azimuth are to a large

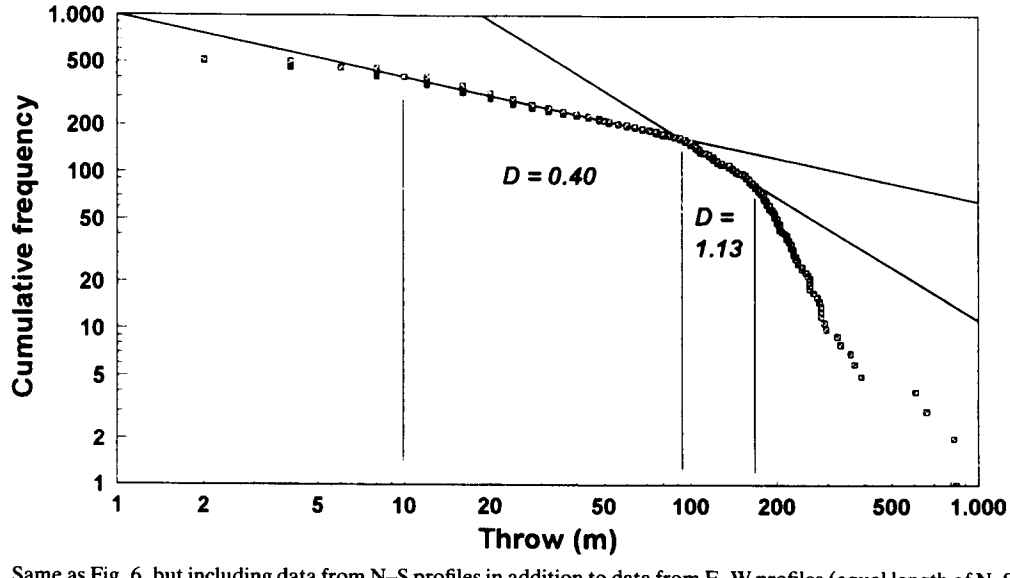

Fig. 7. Same as Fig. 6, but including data from N–S profiles in addition to data from E–W profiles (equal length of N–S and E–W profiles). E–W and N–S oriented faults are thus equally well represented (sampled) in this plot. The lower segment (D = 0.4) is steeper than in Fig. 6. Otherwise the two plots are very similar. See text for discussion.

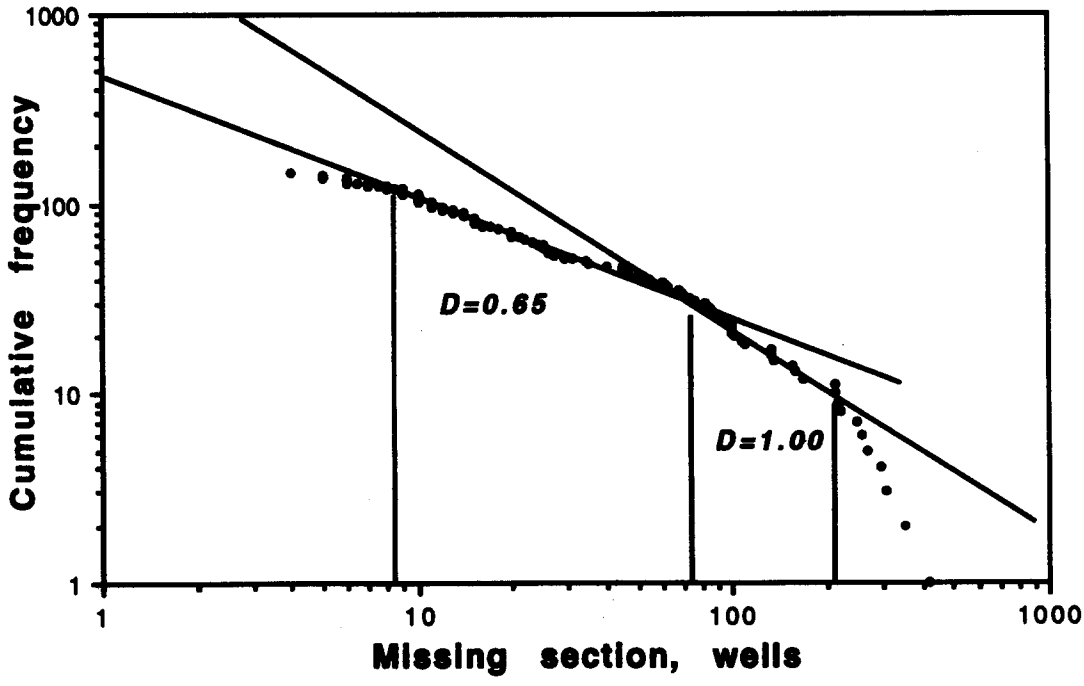

Fig. 8. Cumulative frequency plotted against missing section (in metres), where missing section is estimated from detailed log correlation between wells on the Gullfaks Field. Missing section equals throw if bedding is horizontal. Since bedding generally dips 15° or less, the difference is not substantial. Data from the Upper Triassic–Jurassic sections of all wells on the Gullfaks Field.

extent the same in Figs. 7 and 8, where data were collected along both N–S- and E–W-oriented seismic lines. Furthermore, the differences in dip between seismic and well data sample lines are reduced by the dominant influence of the many long low-angle and horizontal wells through the reservoir. A qualitative, if not quantitative, comparison between Figs. 7 and 8 is therefore possible. The log–log diagram (Fig. 8) shows a segmented curve where a steep portion accounts for the larger (>80 m) fault sizes ($D = 1$) and where a shallower segment ($D = 0.6$–0.7) continues to the left. This is very similar to the diagram shown in Fig. 7 for seismic data, and gives independent evidence for the presence of a break in slope within the seismically resolvable throw range in the Gullfaks Field. Furthermore, the left-hand segment in Fig. 8 extends to throws of only 8–9 m, suggesting that the slope value of −0.3 derived from the seismic data could be safely extrapolated below seismic resolution down to this scale at least.

The results from Figs. 7 and 8 both show that the throw distribution of the entire fault population does not follow a single power-law distribution, even when the orientation sampling effect is corrected for. It is, however, conceivable that the total fault population may contain one or more sub-populations that show simpler power-law distributions. The rest of this section will therefore be concerned with analysis of sub-populations of the faults in the Gullfaks Field. The first natural step would be to sub-divide the population into the geometrically and genetically different domino area, accommodation zone, and horst area. Since data are scarce from the horst complex, no attempt has been made to analyse data from this area.

Domino area

The total fault population in the domino area (sub-population A, Figs. 9 and 10) sampled along E–W lines is not significantly different from the one of the entire study area (Fig. 6). A subdivision of the domino area was therefore necessary.

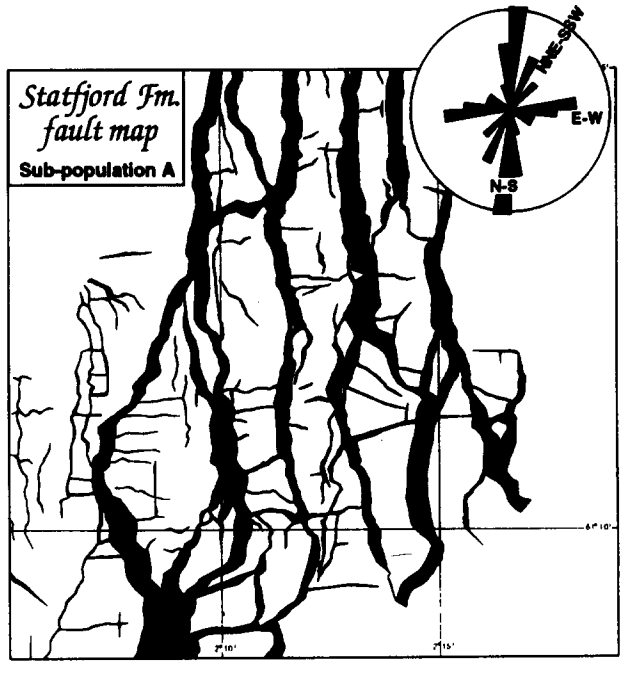

Fig. 9. Faults in the domino area (sub-population A). This population is plotted in Fig. 10. A rose diagram shows the trends of all minor faults (of which most have throw <80 m) of sub-population A (weighted with respect to fault length). A N–S and a E–W set are dominating, with an additional NNE–SSW set of faults.

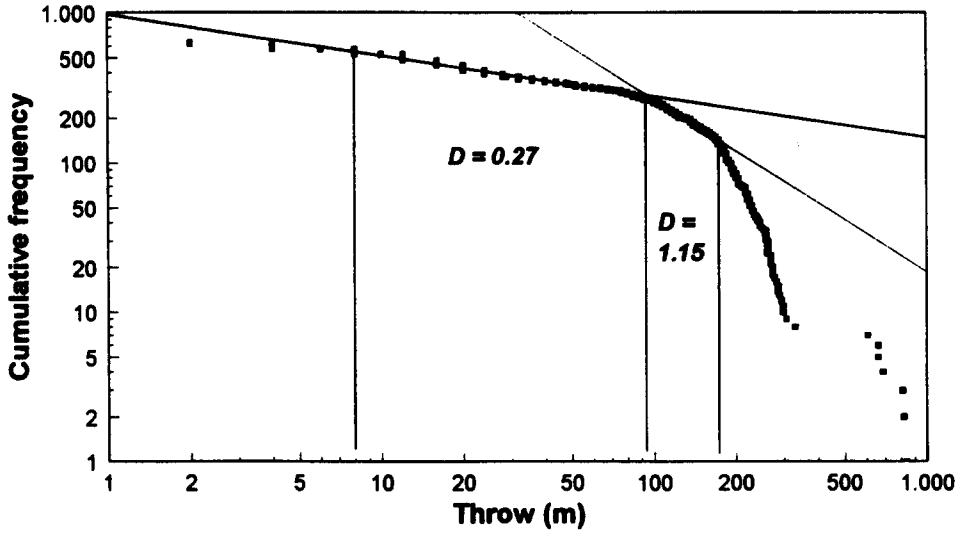

Fig. 10. Cumulative frequency–throw plot of the faults shown in Fig. 9 (measured along E–W lines only at top Statfjord level). The result is very similar to Fig. 6.

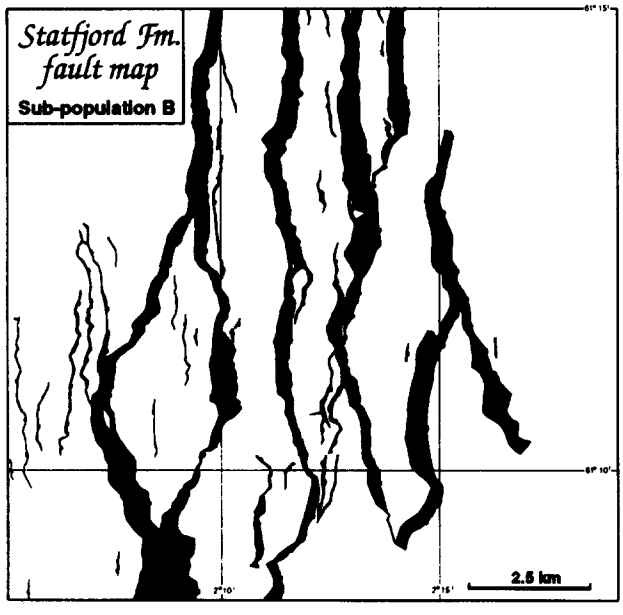

Fig. 11. N–S-striking faults in the domino area (sub-population B) analysed in Fig. 12.

To explore the possibility that N–S-trending main and minor faults together constitute a sub-population that are genetically related, and thus could have a power-law throw distribution, sub-population B (Fig. 11) was analysed. This sub-set is a selection of all approximately N–S-trending faults within the domino area. The result (Fig. 12) is not very different from Fig. 10 or other plots that include the main faults. It seems obvious that the main faults alone or together with any sub-set of the minor faults on the Gullfaks Field can never display a power-law throw distribution. As a consequence of this discovery, we will proceed by studying the throw distribution for individual groups of minor faults.

Minor faults in the domino area can be classified according to their orientation (see rose diagram in Fig. 9). N–S-striking faults (sub-population C, Fig. 13) were measured along E–W lines and plotted in Fig. 14. The result is a curve with a relatively well-defined straight, central segment. The lower cut-off value of this segment occurs at about 20 m. The upper break in slope occurs at

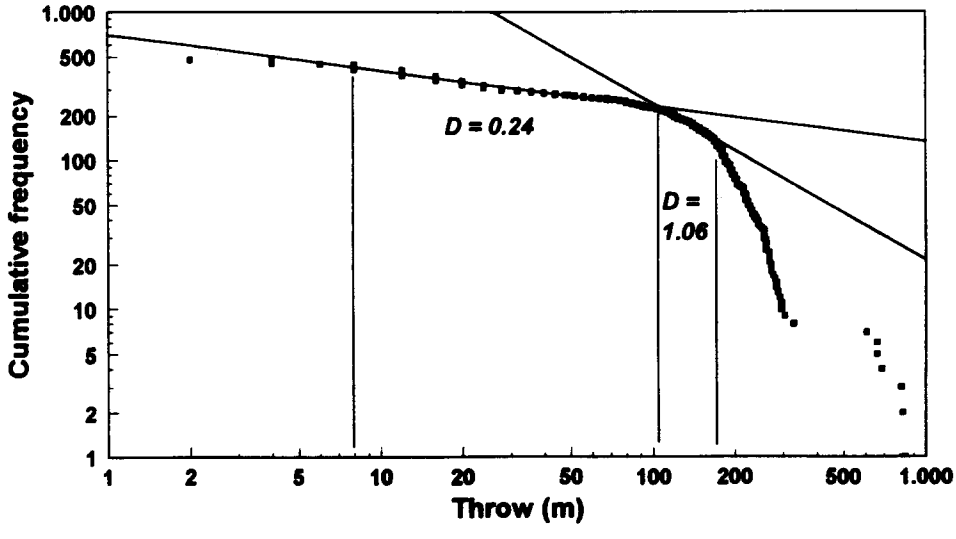

Fig. 12. Cumulative frequency–throw plot of main faults in the domino area (sub-population B, shown in Fig. 11) at top Statfjord level. Two straight lines are shown for reference.

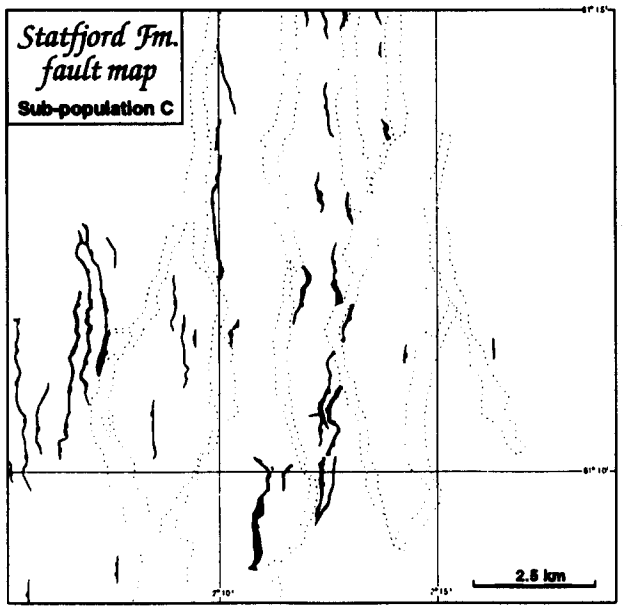

Fig. 13. N–S-striking intra-block faults in the domino area (sub-population C) analysed in Fig. 14.

about 50 m, which represents the maximum throw for most of the N–S faults. Figure 14 altogether displays a curve characteristic of a population with a power-law throw distribution. However, the slope (−2.05) is unrealistically high, and is an effect of removing the main faults from the population.

NNE–SSW-striking faults (sub-population D) occur mainly in the southern and eastern parts of the domino area (Fig. 15). Similar to the N–S minor faults, a power-law throw distribution is indicated (Fig. 16), where an approximately straight portion of the curve is located to the interval 15–100 m. The exponent D (0.73) is, however, much lower than for the N–S fault data (2.05).

The final sub-set of faults investigated in the domino area is faults with strike orientations around E–W (sub-population E, Fig. 17). This sub-population also exhibits a reasonably straight central segment in log–log plots shown in Fig. 18, again indicating a typical power-law distribution above seismic resolution with an exponent of about 1.1.

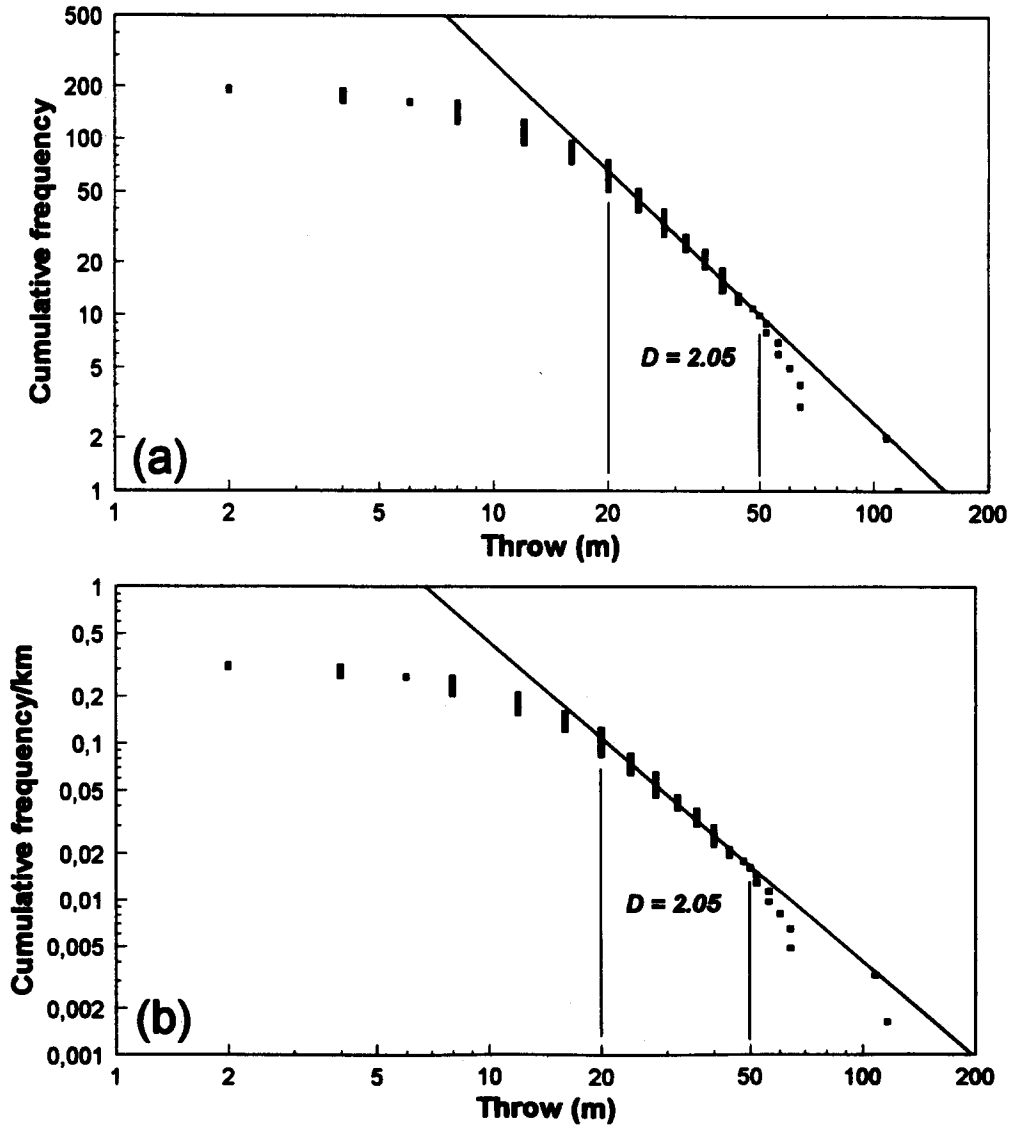

Fig. 14. (a) Cumulative frequency–throw plot of minor, N–S-striking faults in the domino area (population C shown in Fig. 13) at top Statfjord level. (b) Same as (a), but with cumulative frequency km^{-1} as vertical scale, allowing direct comparison with Figs. 16b and 18b.

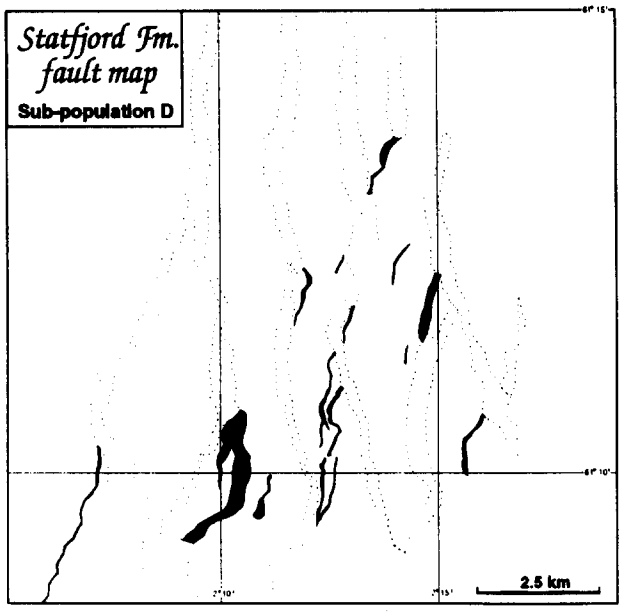

Fig. 15. NNE–SSW-striking minor faults in the domino area, grouped into sub-population D.

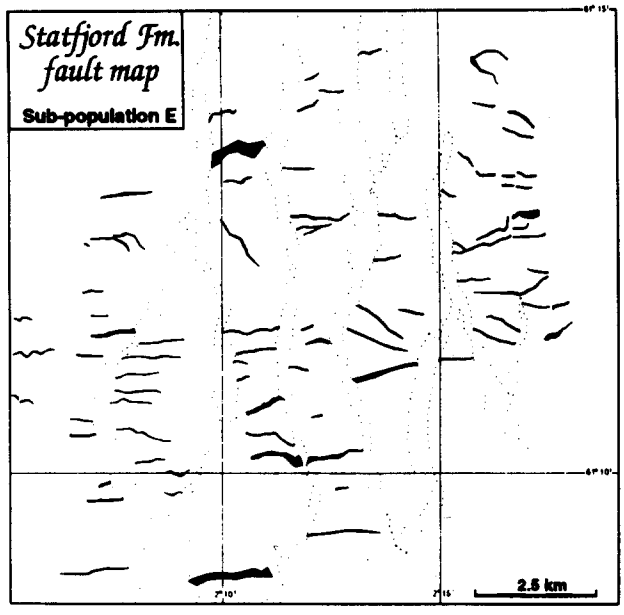

Fig. 17. E–W-striking intra-block faults in the domino area, collectively named sub-population E.

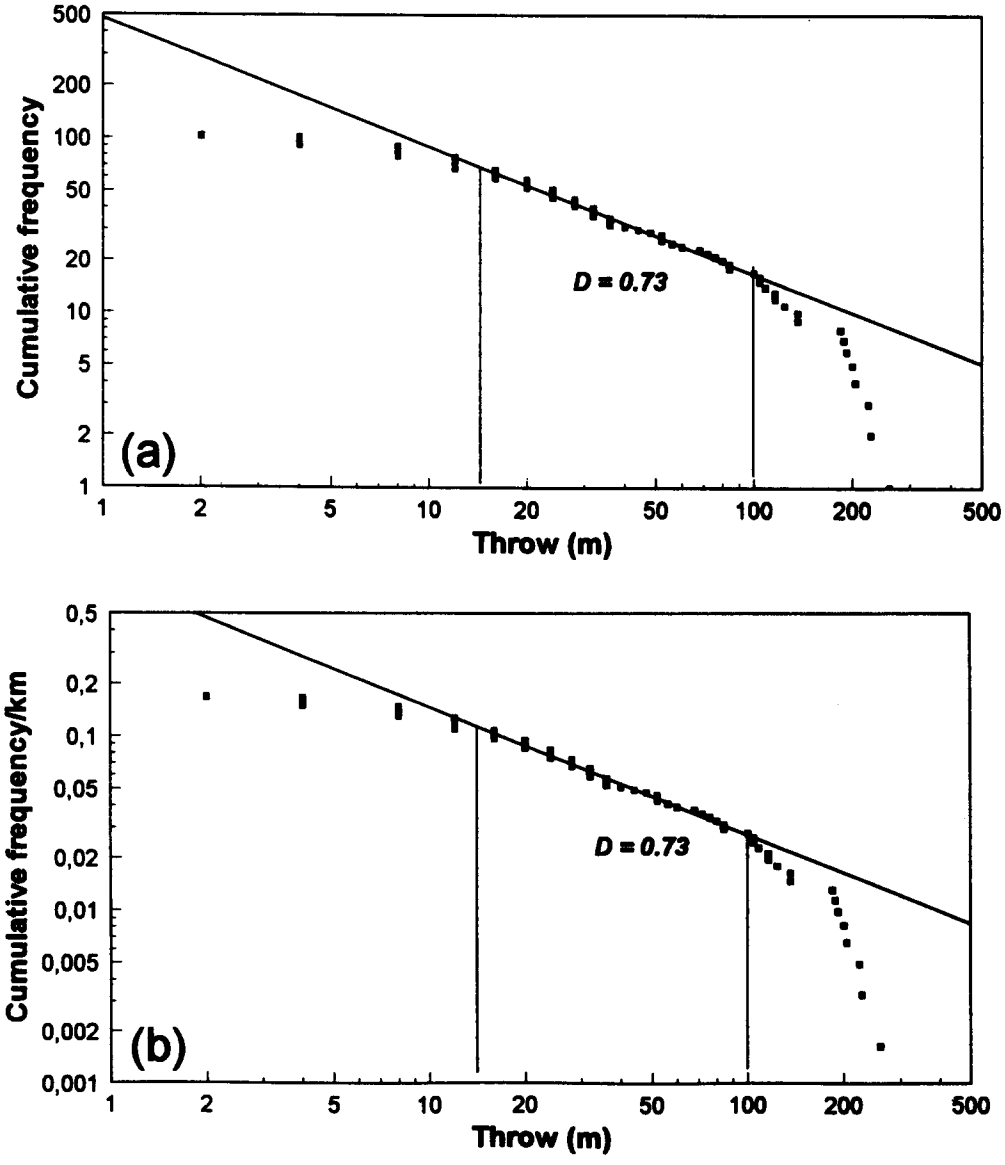

Fig. 16. (a) Cumulative frequency–throw plot of sub-population D (see Fig. 15) in the domino area at top Statfjord level. (b) same as (a), but with cumulative frequency km^{-1} as vertical scale.

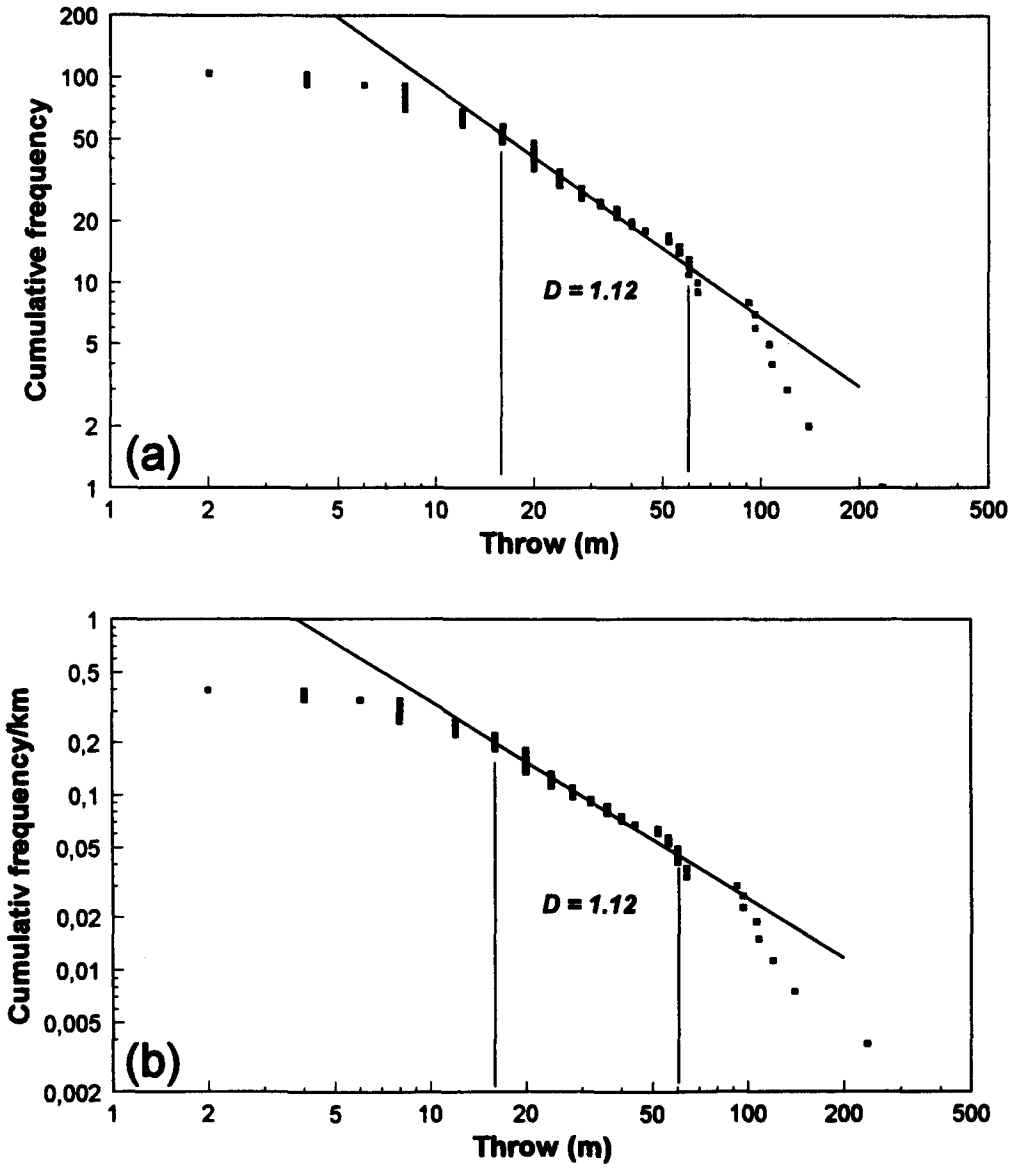

Fig. 18. (a) Cumulative frequency–throw plot of minor, E–W-striking faults in the domino area (population E, shown in Fig. 17) at top Statfjord level. (b) Same as (a), but with cumulative frequency km^{-1} as vertical axis.

Accommodation zone

The majority of the faults in the accommodation zone are related to extension of the outer arc of the gentle fold structure in this zone. The collapse-related fault pattern is better developed at the top Rannoch Formation, and thus data are presented from this level (sub-population F, Fig. 19). The throw data define an approximately straight line segment (power-law exponent of 0.91) in the log–log plots of Fig. 20 for throw values in the range 15–80 m. The other minor faults in this zone are too few for separate analysis.

DISCUSSION AND CONCLUSIONS

It has been shown that even though a total fault population from an area does not show a single power-law size distribution, it may contain sub-populations that do. A trial and error method may be necessary to detect and describe such sub-populations, applying geometric, geographic and/or genetic criteria. In the case of the Gullfaks Field, the minor faults tend to form sub-populations that exhibit power-law throw distributions, whereas the total population shows a segmented throw population curve in log–log plots. The break in slope coincides approximately with the maximum throw value for minor faults (intrablock faults with throws generally <90 m), and most throw values for the main faults are equal to or larger than this value. Segmented, or non-fractal, population curves may in some cases be caused by systematic differences in orientation of small and large faults. On Gullfaks, multiple E–W minor faults in the larger-scale N–S fault system cause an underrepresentation of the lower part of the total population curve. This underrepresentation may be accounted for by combining data collected from two differently oriented sets of profiles, or by the fault trace sampling technique described by Walsh *et al.* (1994). For the case of Gullfaks, however, it was shown that even after removal of

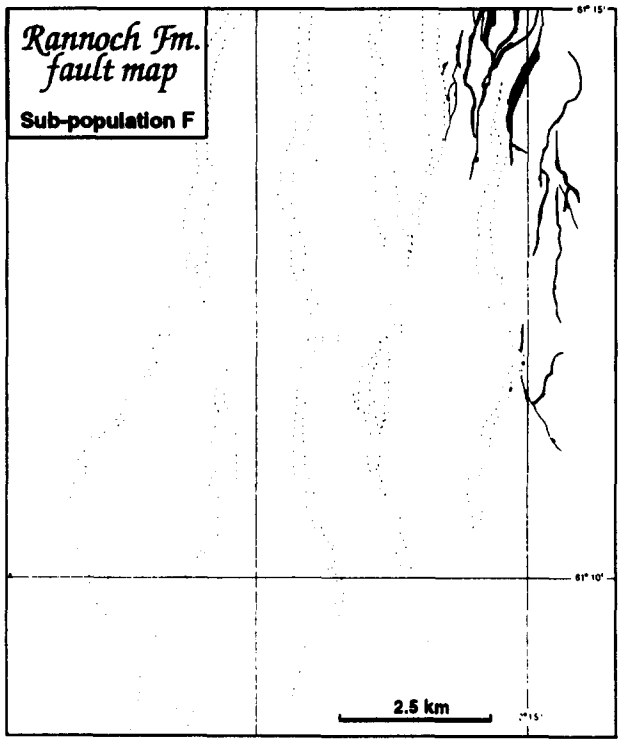

Fig. 19. Faults in the accommodation zone (top Rannoch Formation) thought to be related to extensional collapse of the outer arc of the gentle fold in this area (sub-population F).

this sampling effect, the total fault throw population still did not exhibit self-similar properties. The break in slope is therefore not explained by the difference in orientation between small and large faults, and a simple explanation for this break has not been found.

The sub-populations (minor fault populations) that closely follow a power-law throw distribution show a wide range in exponents (0.73–2.05). These exponents are all higher than the one of the lower (left-hand) segment of the total throw population shown in Fig. 6 ($D = 0.3$). This is mainly an effect of removing the larger faults from the total population, which always leads to a higher exponent (e.g. Jackson & Sanderson 1993). However, the substantial relative differences in exponent emphasizes the impact of subdividing a fault population into sub-groups based on, for example, differences in fault trend.

Extrapolation of linear trends in fault throw population plots to scales below the resolution limit of a particular observational technique has been suggested (e.g. Yielding *et al.* 1992), assuming that fault displacement populations follow scale invariant scaling laws over the displacement range 1 cm–1 km. This assumption may hold true for some populations, but there is no guarantee that it always will. The Gullfaks data (Figs. 6–8) show how fault throw population curves may be segmented. If the break in slope recognized for the Gullfaks data occurred below seismic resolution, extension of the right-hand central segment (D-value about 1) would have lead to a gross overestimate of small faults. Independent field data show that such breaks in slope do occur below what is normally considered to be seismic resolution. For instance, Brodahl (1993) demonstrated that the total fault population (0.2–70 m displacement) in the northern Somerset area shows a straight segment when plotted on a throw population plot, but that a break in slope occurs at about 5 m. This break is well above the resolution of the field data collected from the area, but below seismic resolution. Hence, extrapolations below seismic resolution may lead to serious overestimates of the sub-seismic fault throw distribution, fault density and total extension.

For the case of Gullfaks, well data suggest that extrapolations may be justified over the interval 8–80 m, but the potential for sub-seismic breaks occurring below 8 m of throw is still unconstrained. The danger of extrapolating linear trends in fault population plots into the sub-seismic field in oil fields like Gullfaks is to predict an unrealistically high density of small faults in the reservoir. An extrapolation can therefore in many

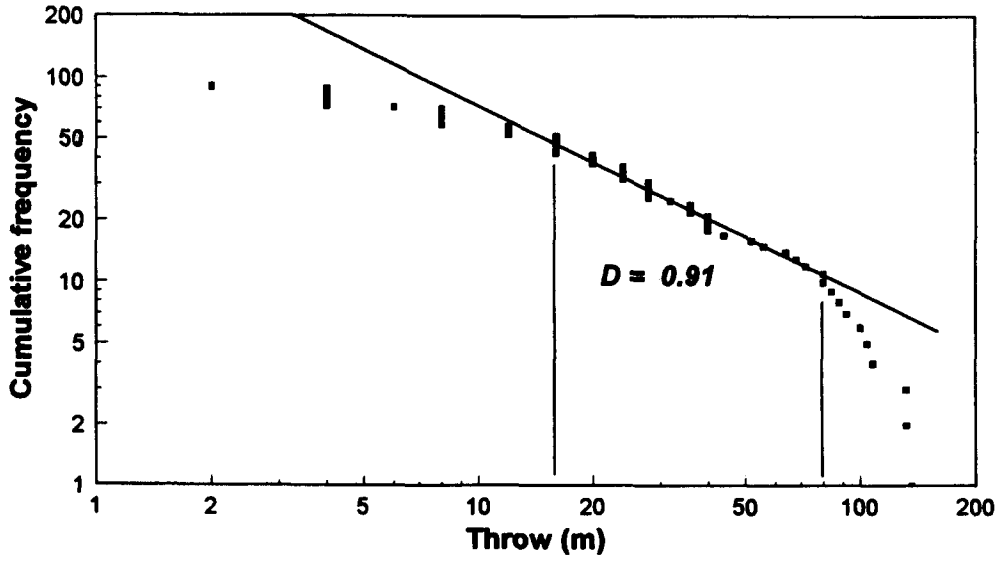

Fig. 20. Cumulative frequency–throw plot of sub-population F from the accommodation zone, shown in Fig. 19 for top Rannoch Formation.

cases at the best be considered a maximum estimate of the small-scale faulting.

Acknowledgements—Steve Knott and Tim Needham are thanked for constructive and helpful reviews, which together with additional comments by P. Cowie significantly improved the text. R. Hansen, J. Henden, J. Hesthammer and A. Thon helped in the seismic interpretation used in this study. We thank Norsk Hydro a.s., Sage Petroleum a.s. and Statoil for permission to publish these results.

REFERENCES

Badley, M. E., Price, J. D., Dahl, C. R. & Agdestein, T. 1988. The structural evolution of the northern Viking Graben and its bearing upon extensional modes of basin formation. *J. geol. Soc. Lond.* **45**, 455–472.

Brodahl, E. 1993. Forkastningsmønster i nord Somerset. Unpublished thesis, Norwegian Institute of Technology, Trondheim.

Childs, C., Walsh, J. J. & Watterson, J. 1990. A method for estimation of the density of fault displacements below the limits of seismic resolution in reservoir formations. In: *North Sea Oil and Gas Reservoirs—II* (edited by Buller, A. T., Berg, E., Hjelmeland, O., Torsaeter, O. & Aasen, J. O). Graham & Trotman, London, 309–318.

Erichsen, T., Helle, M., Henden, J. & Rognebakke, A. 1987. Gullfaks. In: *Geology of the Norwegian Oil and Gas Fields* (edited by Spencer, A. M., Campbell, C. J., Hauslien, S. H., Nelson, P. H., Nysæther, E. & Ormaasen, E. G.). Graham & Trotman, London, 283–286.

Fossen, H., 1992. The nature and significance of extensional tectonics in the Caledonides of South Norway. *J. Struct. Geol.* **14**, 1033–1046.

Gauthier, B. D. M. & Lake, S. D. 1993. Probabilistic modeling of faults below the limit of seismic resolution in Pelican Field, North Sea, offshore United Kingdom. *Bull. Am. Ass. Petrol. Geol.* **77**, 761–777.

Hirata, T. 1989. Fractal dimension of fault systems in Japan: fractal structure in rock fracture geometry at various scales. *Pure & Appl. Geophys.* **131**, 157–170.

Jackson, P. & Sanderson, D. J. 1993. Scaling of fault displacements from the Badajoz-Cordoba shear zone, SW Spain. *Tectonophysics* **210**, 179–190.

Kojima, K., Tosaka, H. & Ohno, H. 1989. An approach to wide-ranging correlation of fracture distributions using the concept of fractal. In: *Rock Mechanics as a Guide for Efficient Utilization of Natural Resources* (edited by Khair). Balkema, Rotterdam, 211–218.

Marrett, R. & Allmendinger, R. W. 1992. Amount of extension on "small" faults: an example from the Viking Graben. *Geology* **20**, 47–50.

Marsden, G., Yielding, G., Roberts, A. M. & Kusznir, N. J. 1990. Application of a flexural cantilever simple-shear/pure shear model of continental lithosphere extension to the formation of the northern North Sea basin. In: *Tectonic Evolution of the North Sea Rifts* (edited by Blundell, D. J. & Gibbs, A. D.). Clarendon Press, Oxford, 241–261.

Peacock, D. C. P. & Sanderson, D. J. 1994. Strain and scaling of faults in the chalk at Flamborough Head, U.K. *J. Struct. Geol.* **16**, 97–107.

Petterson, O., Storli, A., Ljosland, E. & Massie, I. 1990. The Gullfaks Field: geology and reservoir development. In: *North Sea Oil and Gas Reservoirs — II* (edited by Buller, A. T., Berg, E., Hjelmeland, O., Kleppe, J., Torsoeter, O. & Aasen, J. O.). Graham & Trotman, London, 67–90.

Roberts, A. M., Yielding, G. & Bradley, M. E. 1990. A kinematic model for the orthogonal opening of the late Jurassic North Sea rift system, Denmark Mid Norway. In: *Tectonic Evolution of the North Sea Rifts* (edited by Blundell, D. J. & Gibbs, A. D.). Clarendon Press, Oxford, 180–199.

Roberts, A. M., Yielding, G., Kusznir, N. J., Walker, I. M. & Dorn-Lopez, D. 1995. Quantitative analysis of Triassic extension in the northern Viking Graben. *J. geol. Soc. Lond.* **152**, 15–26.

Scott, D. L. & Rosendahl, B. R. 1989. North Viking Graben: an east African perspective. *Bull. Am. Ass. Petrol. Geol.* **73**, 155–165.

Walsh, J. J. & Watterson, J. 1987. Distributions of cumulative displacement and seismic slip on a single normal fault surface. *J. Struct. Geol.* **9**, 1039–1046.

Walsh, J., Watterson, J. & Yielding, G. 1991. The importance of small-scale faulting in regional extension. *Nature* **351**, 391–393.

Walsh, J. J., Watterson, J. & Yielding, G. 1994. Determination and interpretation of fault size populations: procedures and problems. In: *North Sea Oil and Gas Reservoirs — III* (edited by Aasen, J. O., Berg, E., Buller, A. T., Hjelmeland, O., Holt, R. M., Kleppe, J. & Torsæter, O.). Kluwer, Dordrecht, 141–155.

Yielding, G., Walsh, J. & Watterson, J. 1992. The prediction of small-scale faulting in reservoirs. *First Break* **10**, 449–460.